Combustion and Flame 190 (2018) 188–200

Contents lists available at ScienceDirect

Combustion and Flame

journal homepage: www.elsevier.com/locate/combustflame

Influence of potassium chloride and other metal salts on soot formation studied using imaging LII and ELS, and TEM techniques

Johan Simonsson*, Nils-Erik Olofsson, Ali Hosseinnia, Per-Erik Bengtsson

Division of Combustion Physics, Department of Physics, Lund University, P.O. Box 118, SE-221 00 Lund, Sweden

ARTICLE INFO

Article history:
Received 27 June 2017
Revised 7 August 2017
Accepted 21 November 2017
Available online 22 December 2017

Keywords:
Laser-induced incandescence
Elastic light scattering
Particle size
Potassium
Soot
Alkali metals

ABSTRACT

An experimental investigation has been performed where the influence of metal salts on soot formation has been studied. By combining two-dimensional laser-induced incandescence (LII) and elastic light scattering (ELS), two-dimensional information could be obtained on soot properties in the flames. For these studies, seven metal salts (NaCl, $MgCl_2$, $AlCl_3$, KCl, $CaCl_2$, $FeCl_3$ and $ZnCl_2$) were dissolved in water and aspirated into a premixed ethylene/air flame. At lower flame heights, in the soot inception region, the LII signal (representing soot volume fraction) was marginally affected by all additives, whereas the ELS signal strongly decreased with increasing additive concentration for the alkali salts. At higher heights, in the soot growth region, the soot volume fractions were lowered for the addition of potassium, calcium and sodium chloride, in order of significance. Some of the salts ($MgCl_2$, $AlCl_3$ and $FeCl_3$) resulted in negligible influence on LII signals and slightly higher ELS signals throughout the flames, and we relate the increased ELS signals to salt particles propagating through the flame. Main focus in our study was on the addition of potassium chloride for which several parameters were investigated. For example, soot primary particle sizes were evaluated using combined LII and ELS, showing decreasing particle sizes for increasing concentrations of potassium, in reasonable agreement with particle sizes evaluated using transmission electron microscopy. Also, CARS thermometry showed slightly higher flame temperature, ~30 K, for the potassium-seeded flame compared to the reference flame.

1. Introduction

Soot emissions are known to have negative impact on human health [1] as well as on environment and climate [2]. A serious climatological effect is global warming, and knowledge on the impact of soot on this phenomenon has increased in recent years. Soot is now believed to be one of the main contributors, along with carbon dioxide and methane, to global warming [2,3]. This effect is mainly combustion-related due to the extensive use of fossil fuels. The future direction globally is toward replacing fossil fuels with renewable sources, e.g. by using biomass fuels in combustion and gasification. These fuels, however, show large variation in concentration of ash-forming compounds, of which metal compounds constitute the major part. For example, stem wood has low concentrations of these compounds. Bark, on the other hand, has metal concentrations of several percent [4]. The influence of various metals on the soot formation may, at least partly, explain why gasification of different biomass sources lead to various soot concentration levels under the same fuel-to-air ratios [5]. Hence it is of great interest to gain better understanding of the role of metal compounds in soot formation processes. In order to gain basic knowledge on characteristics in real-world gasifiers, simplified laboratory systems such as premixed and non-premixed flames can give valuable information, which is not distinguishable in large scale experiments.

It is well-known, since the middle of the last century, that metal additives could have a pronounced effect on soot formation [6]. In the subsequent decades after this observation, different additives were tested in gas turbines [7] as well as in diesel engines [8], and depending on the additive used, soot formation could be either promoted or reduced. One of the earliest systematic investigations with metal salts and salt solutions introduced to sooting flames was presented in 1971 by Cotton et al. [9]. In this work they investigated propane diffusion flames using gravimetric soot sampling and direct observations of flame height. The results showed that especially alkali and alkaline earth metals decrease the amount of soot significantly. In the following year, Salooja et al. [10] presented results based on sampling showing inhibition of carbon formation when metals were placed in the reaction zone of the investigated flame. In 1975, Bulewicz et al. [11] investigated the effect of metal additives on soot formation in diffusion flames

* Corresponding author.
E-mail address: johan.simonsson@forbrf.lth.se (J. Simonsson).

https://doi.org/10.1016/j.combustflame.2017.11.020
0010-2180/

of acetylene and propane using gravimetric sampling for soot concentration and TEM for particle sizing. They suggested that ionic species rather than neutral ones were responsible for the observed effects of either soot promotion or soot reduction.

The first measurements investigating the influence of salts on soot formation using optical diagnostics were presented by Haynes et al. in 1979 [12] for premixed ethylene flames and in 1981 for premixed benzene flames [13]. In these studies, soot concentration and particle sizes were evaluated from combined elastic light scattering and extinction measurements. In the paper from 1979, Haynes et al. showed that introducing alkali metals (Na, K, and Cs) to the flame significantly reduced the scattered light, where cesium showed the strongest effect, followed by potassium and then sodium. In comparison to the scattering measurements, the extinction measurements only showed small variations when adding alkali metals. By combining the data from extinction and scattering measurements, they concluded that particle sizes decreased markedly with increased concentration of the additive, especially for potassium. Of the investigated alkaline earth metals (Ba, Sr and Ca), only additives of barium to the sooting flame led to the same strong soot suppression effects as the alkali metals, while the additives strontium and calcium led to a decrease in scattering of the same magnitude as the decrease in extinction. Similar measurements were performed in benzene flames seeded with a variety of metals including several alkali and alkaline earth metals [13]. The results showed the same trends as for the measurements performed in ethylene flames.

In a review paper by Howard and Kausch [14] from 1980, they discuss three main mechanisms for how different additives impact the soot formation in flames. The first mechanism, also known as an ionizing mechanism, occurs mostly for metals which ionize significantly in the flame due to their low ionization potential, e.g. sodium and potassium. It is speculated that this ionization may lower the coagulation and nucleation rates resulting in lower soot concentrations and smaller sizes. Investigations of additives showing behavior according to the first mechanism can be found in, for example, the work presented earlier by Haynes et al. [12] and also by Bonczyk et al. in [15,16]. For example, Bonczyk [16] shows a clear correlation between decreasing particle sizes and lower ionization potential in his studies using various alkali additives. In the second mechanism presented in [14], the additives together with the flame gases create hydroxyl radicals which lower the amount of soot and precursors of soot. The second mechanism affects the flame for additives such as barium, calcium and strontium. Measurements in flames using, e.g., calcium and barium additives have been performed both by Haynes et al. [12] and by Bonczyk et al. [17] showing decreased concentrations of soot. The third mechanism affects the soot formation in flames when metals such as manganese, iron, cobalt, and nickel, are used. These metals are speculated to increase the oxidation rate of soot late in the flame (secondary flame zone). Only marginal effects are often found in the primary flame zone.

It is not certain that a specific metal always affects soot formation in a distinct way, since the effect may be related to, for example, flame type and in what configuration the metal is introduced to the flame. As an example, in studies of iron additives to flames, the effect on soot formation has depended strongly on how the iron atom was bonded in a molecule before entering the flame, see for example [18–22]. In a TEM study conducted by Wong [19], it was found that ferrocene only had a marginal influence in reducing the particle sizes of the soot, while ferric acetylacetonate significantly reduced the soot particle sizes. In work by Hahn and Charalampopoulos [20], where they studied the effect of iron pentacarbonyl additive, they conclude that iron will nucleate as iron oxide prior to soot inception and thereby provide a location for soot inception and deposition, which could explain the measured increase in soot concentration found. Feitelberg et al. [22] also showed results from extinction and scattering measurements that indicate an increase in soot volume fractions for added ferrocene. They discuss why well known soot suppressors, such as iron and manganese, could result in an increased soot concentration. A plausible explanation is that initially when the flame is fuel-rich, the additives may increase the amount of soot, while it can catalyze the soot oxidation later in the flame.

In the present work the influence on the soot formation of seven metal salts aspirated into a premixed ethylene/air flame has been investigated, where a limited part was presented previously [23]. The work focuses on the use of advanced optical methods, and for the first time laser-induced incandescence (LII) has been used for study of the influence of additives on soot formation. The LII technique allows extraction of two-dimensional information of soot volume fractions. Also elastic light scattering (ELS), extinction measurements, and transmission electron microscopy (TEM) have been used, the latter to study the morphology of sampled soot. In our previous paper by Simonsson et al. [23], we presented results from laser measurements showing a significant decrease in soot volume fraction when adding potassium chloride, while there was only a marginal influence, a slight increase, on the soot volume fraction resulting from adding iron (III) chloride to the flame. The optical results indicated that the soot particles were smaller for the potassium-seeded flames, which were also supported by TEM measurements. In the present paper, more extensive results are presented from the seeding of all seven salts along with further evaluation of the results of potassium chloride. For the potassium chloride-seeded flames we present evaluated soot primary particle sizes based on combined LII and ELS measurements, and a discussion of how measurements of the depolarization scattering ratio can be used to estimate the influence of fluorescence from PAHs and soot precursors on the ELS signal. Furthermore, measurements by coherent anti-Stokes Raman spectroscopy (CARS) were performed to study the influence of potassium on the flame temperature. We also discuss scattering effects from the salt particles themselves as well as study the soot oxidation effects caused by the more diffusion-like flame at the edges of the investigated premixed flame.

2. Theoretical considerations

In this work, mainly three laser diagnostic techniques have been used; laser-induced incandescence (LII), elastic light scattering (ELS) and extinction. In this section, these techniques will be briefly described and some theory needed for evaluation will be presented.

Laser-induced incandescence is a technique for soot concentration measurements, where the energy of the incident laser pulses is absorbed by soot particles, resulting in an increase in temperature to about 4000 K and thereby also increase of the Planck radiation [24,25]. This increased Planck radiation from the heated soot on top of the natural flame luminosity is called the LII signal. The LII signal has been shown to be approximately proportional to the soot volume fraction when applied in flames [26]. However, using LII by itself cannot measure quantitative soot volume fractions without being calibrated using a secondary technique. In the present work, extinction has been used to calibrate the LII signal to soot volume fractions. LII can also be used for temperature measurements using 2-color pyrometry [27], and for particle size measurements from fitting of experimental LII signal decay curves using theoretically modeled curves [28,29].

Extinction is a line-of-sight technique, where the laser intensity attenuation, in this case caused primarily by absorption in soot particles, is measured. The initial intensity, I_0, and the transmitted intensity, I, can be used to evaluate the extinction coefficient,

K_{ext}, using the Beer–Lambert law, $I = I_0 e^{-K_{ext}L}$, where L is the absorption length. By assuming that the primary soot particles are spherical and the measurements take place within the Rayleigh limit, i.e. that the soot particles are much smaller than the incident laser wavelength, then it is common practice to neglect the scattering contribution to the extinction, i.e., the absorption coefficient, K_{abs}, is equal to the extinction coefficient. However, if the particles start to aggregate and reach larger sizes, this assumption may be violated. For soot particles and aggregates of arbitrary size and shape, the theory of absorption and scattering is complex and calculations do often require numerical approaches [30–32]. The Rayleigh–Debye–Gans (RDG) approximation can often be used with satisfactory accuracy [33]. In this approximation, the absorption cross section is given by the absorption cross section for the individual soot particles multiplied by the number of soot particles per aggregate. The absorption will therefore be expected to be volume dependent, which is a reality in the Rayleigh limit. The expression for the absorption coefficient valid in the Rayleigh limit, should therefore also be valid in the RDG approximation. The absorption coefficient according to Rayleigh theory for isotropic spheres is defined according to:

$$K_{abs}(=K_{ext}) = -\frac{\pi^2}{\lambda}\mathrm{Im}\left(\frac{m^2-1}{m^2+2}\right)Nd^3. \quad (1)$$

where, λ is the laser wavelength, m is the complex refractive index, N is the particle number concentration, and d is the primary particle diameter of the soot [30]. The factor $-\mathrm{Im}(\frac{m^2-1}{m^2+2})$ is often denoted $E(m)$ which will be used from this point forward. The soot volume fraction, f_v, is defined:

$$f_v = N\frac{\pi d^3}{6}. \quad (2)$$

By combining Eqs. (1) and (2) and the Beer–Lambert law, the following expression can be derived from which the soot volume fraction can be calculated based on the experimentally measured extinction coefficient;

$$f_v = \frac{K_{ext}\ \lambda}{6\pi\ E(m)}. \quad (3)$$

The third technique used is elastic light scattering, which is a technique where the scattered light intensity at the same wavelength as the laser wavelength is measured. In this work, all scattering results are presented as Q_{vv}-factors (unless otherwise stated), where the "v" represents the polarization of the measured and incident light, in this case both vertical. The Q_{vv} factor can for non-aggregated particles [31,34] be expressed as:

$$Q_{vv} = N\left(\frac{2\pi}{\lambda}\right)^4\left(\frac{d}{2}\right)^6\left|\frac{m^2-1}{m^2+2}\right|^2. \quad (4)$$

The factor $|\frac{m^2-1}{m^2+2}|^2$ is sometimes referred to as $F(m)$, which is the expression that will be used further on in the present paper. If particle aggregation is taken into account, then Eqs. (2) and (3) have to take the number aggregate concentration, N_a, and the number of primary particles per aggregate, n, into account according to RDG-theory [31] giving the new expressions:

$$Q_{vv} = N_a n^2\left(\frac{2\pi}{\lambda}\right)^4\left(\frac{d}{2}\right)^6\left|\frac{m^2-1}{m^2+2}\right|^2 S(q) \quad (5)$$

$$f_v = N_a n\frac{\pi d^3}{6} \quad (6)$$

where $S(q)$ is the structure factor of the aggregate. The structure factor is described by different expressions depending on size and magnitude of the scattering wave vector. In the Rayleigh, Guinier and power law regimes respectively, the structure factor is described according to:

$$S(q) = 1 \quad qR_g \ll 1 \quad (7a)$$

$$S(q) = 1 - \frac{q^2R_g^2}{3} \quad qR_g \lesssim 1 \quad (7b)$$

$$S(q) = C(qR_g)^{-D_f} \quad qR_g > 1 \quad (7c)$$

where R_g is the radius of gyration, and $\vec{q}$ is the scattering wave vector, where the inverse of q represents the length scale of the scattering experiment. C represents a coefficient determining the cut-off level between the Guinier and power law regime and D_f is the fractal dimension. For further discussion regarding scattering theory and background reading, see a review by Sorensen [31].

From Eq. (2) it is clear that the LII signal, which is proportional to the soot volume fraction, has a power dependence of three to the primary particle diameter. For the ELS signal, Eq. (4), the power dependence of the particle diameter is six, which makes ELS much more sensitive to changes in particle sizes. By combining either Eqs. (2) and (4), or Eqs. (5) and (6), depending on whether aggregation is taken into account, it is possible to derive particle sizes from the combined LII and ELS measurements. More information on measurements and evaluation performed using this method can for example be found in [35,36].

3. Experimental setup

In Fig. 1 the experimental setup (Fig. 1a) is presented along with an image of the reference flame (Fig. 1b) and an image of the burner head (Fig. 1c). The setup consisted of two laser systems, one Nd:YAG laser (Quantel Brilliant B) together with a frequency doubling unit for the LII and ELS measurements and one diode laser giving a laser beam at a wavelength of 850 nm for the extinction measurements. The LII measurements were performed using the fundamental output of the Nd:YAG laser at 1064 nm for heating the soot particles and thereby inducing the LII signal, which was collected using an ICCD-camera with a short-pass filter placed in front with a cut-off wavelength of 425 nm. For the ELS measurements the second harmonic of the Nd:YAG laser at 532 nm was used. The same camera was used for detecting the elastic light scattering at 532 nm, however the short-pass filter was here replaced by a polarizer, an interference filter with transmission at 532 nm (FWHM: 2.5 nm), and optionally neutral density (ND) filters with suitable optical density to maximize the dynamic range of the camera. The measurements of LII and ELS were not performed simultaneously, which is acceptable as the flame is very stable. The laser beam not in use was blocked using a beam dump when the other laser beam was used for measurements.

Calibration of the LII signals to soot volume fractions was performed as described in relation to Eq. (3) using extinction measurements. A diode-laser wavelength of 850 nm was selected in the infrared spectral region to avoid absorption by polycyclic aromatic hydrocarbons [37]. The absorption function, $E(m)$ was set to 0.35 according to our previous work in similar flames [38,39]. It has been shown that $E(m)$ in this type of sooting flame increases with flame height as the soot becomes more mature, however, $E(m)$ and its variation in the present flame is not known, and we have set $E(m)$ to 0.35 as this is the most relevant choice. However, any choice of $E(m)$ introduces uncertainties in the estimation of soot volume fraction as discussed in Section 4.3. For calibration of the ELS signals from soot, the ELS signals from pure nitrogen were measured at 295 K and atmospheric pressure, for which the scatter factor, Q_{vv}, is measured to be 1.55×10^{-6} $m^{-1}sr^{-1}$ at 532 nm [40].

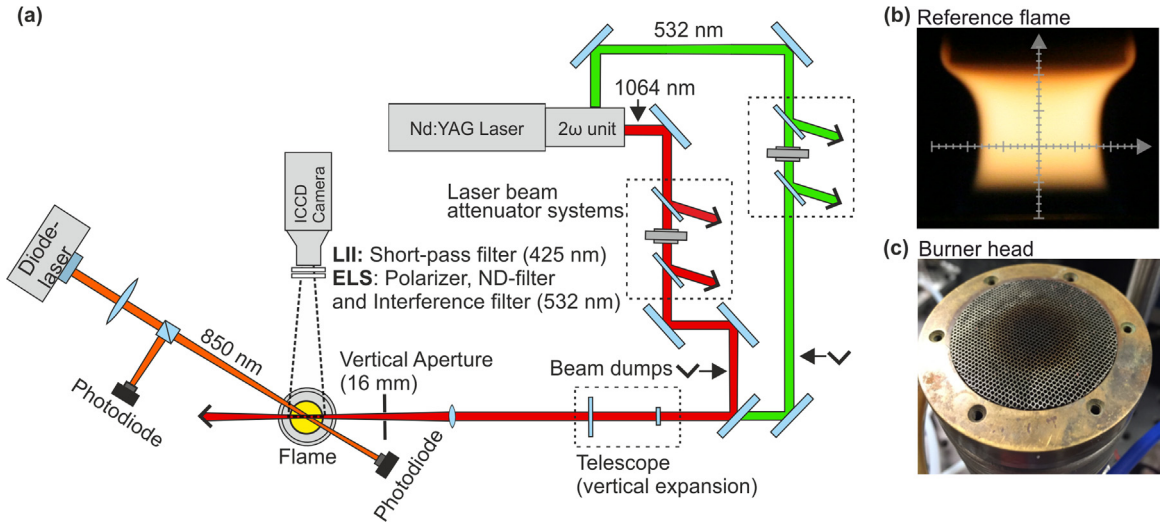

Fig. 1. (a) Sketch of the experimental setup used during the experiments and (b) an image of the reference flame with an overlapped mm-grid and (c) a photo of the burner head.

For further information regarding the present setup, see our previous publication [23]. For more detailed information regarding the LII and ELS setup, see for example [25,38], and for detailed discussion regarding the extinction measurements, see [37], where sensitivity and accuracy of the extinction measurements are discussed.

The measurements were performed in a premixed ethylene/air flame on a modified PerkinElmer burner, which can be seen in Fig. 1c. This is a water-cooled burner where the fuel, oxidizer and co-flow passes through a mesh with holes of approximately 1 mm in diameter and depth of 20 mm. The mesh has ha diameter of 45 mm, which includes both the flame region and the co-flow region. The center part, i.e. where the premixed ethylene/air passes the mesh has a diameter of 23 mm. More details about the burner can be found in [41]. The flame was operated with an equivalence ratio, $\phi = 2.6$. The flow of ethylene was set to 0.27 l/min and the flow of air was set to 1.5 l/min. These flows are defined for 273 K and 1 atm. A co-flow of air was introduced around the flame, with a flow of 5 l/min to increase stability. A flame stabilizer of stainless steel was placed with its lower edge at a height of 21 mm above the burner surface.

The modified PerkinElmer burner allows seeding of various solutions in the oxidant air. The solution carried by the oxidant air comes in contact with an impact bed and a flow spoiler, which only allows small aerosols to the burner head. For more details and images regarding the seeding procedure, see [41]. In the present work, the solutions consisted of either distilled water (for the reference flame) or distilled water with various added metal salts at different concentrations (0.01 M, 0.1 M and 1 M). The investigated salts were NaCl, $MgCl_2$, $AlCl_3$, KCl, $CaCl_2$, $FeCl_3$ and $ZnCl_2$ and the amount of solution seeded into the flame was approximately 3 ml per h. For a 1 M salt solution, this corresponds to a salt concentration of $\sim 1.7 \times 10^{16}$ cm^{-3}, which is equivalent to approximately 700 ppm in the flame.

The soot samples studied using transmission electron microscopy (TEM) were collected inside the flame using carbon-coated copper grids attached to a pneumatic probe. The residence time for the probe inside the flame was approximately 100 ms, and the soot was collected based on thermophoresis. The samples were then evaluated in a TEM microscope (FEI Tecnai Spirit BioTWIN), which has a magnification factor up to 300.000. The evaluation of the TEM images was accomplished manually by measuring the size of the primary particles calibrated with the scale given by the TEM microscope software.

4. Results and Discussion

When discussing the results for the studied flames, four different spatial regions will be used to simplify the discussions. The flame regions are denoted in the following way; the pre-reaction region (0–2 mm HAB), the pre-soot region (2–4 mm HAB), the soot inception region (4–8 mm HAB), and finally the soot growth region (8–17 mm HAB). HAB is the acronym for height above burner.

4.1. Two-dimensional LII and ELS

To illustrate the kind of results we obtain and show the impact on the flame when salt solutions, in this case 0.01 M, 0.1 M, and 1 M KCl, are added, eight images are shown in Fig. 2. In the first and second row, the LII signal calibrated to soot volume fractions and the elastic light scattering as Q_{vv}-factor are shown, respectively, for the entire width of the flame from a height above burner of 0 to 17 mm. In these graphs with two-dimensional information, it is clear that the entire flame is affected by the seeded KCl solution, and most obvious for the ELS measurements where the signal decreases significantly. In the following sections, more detailed information is given on how the LII and ELS signal change along the centerline of the flames, and comparisons how the seven salts influence the flame.

4.2. LII and ELS signals for all additives at 10 mm HAB

Figure 3 summarizes the results at 10 mm HAB along the centerline of the flame by showing normalized LII and ELS signals for all the salts. The results are normalized to measurements in the reference flame also performed at 10 mm HAB. The measurements were conducted sequentially with distilled water and salt solutions of 0.01 M, 0.1 M, and 1 M. This sequence was repeated three times for each salt, and the data in Fig. 3 are averaged for the three measurements conducted for each case.

Based on the results from the LII measurements presented in Fig. 3, it is clear that most of the flames are marginally affected by adding salt solutions when it comes to soot volume fraction (as the LII signal is approximately proportional to the soot volume fraction). However, we can see a clear decrease in LII signal for all KCl

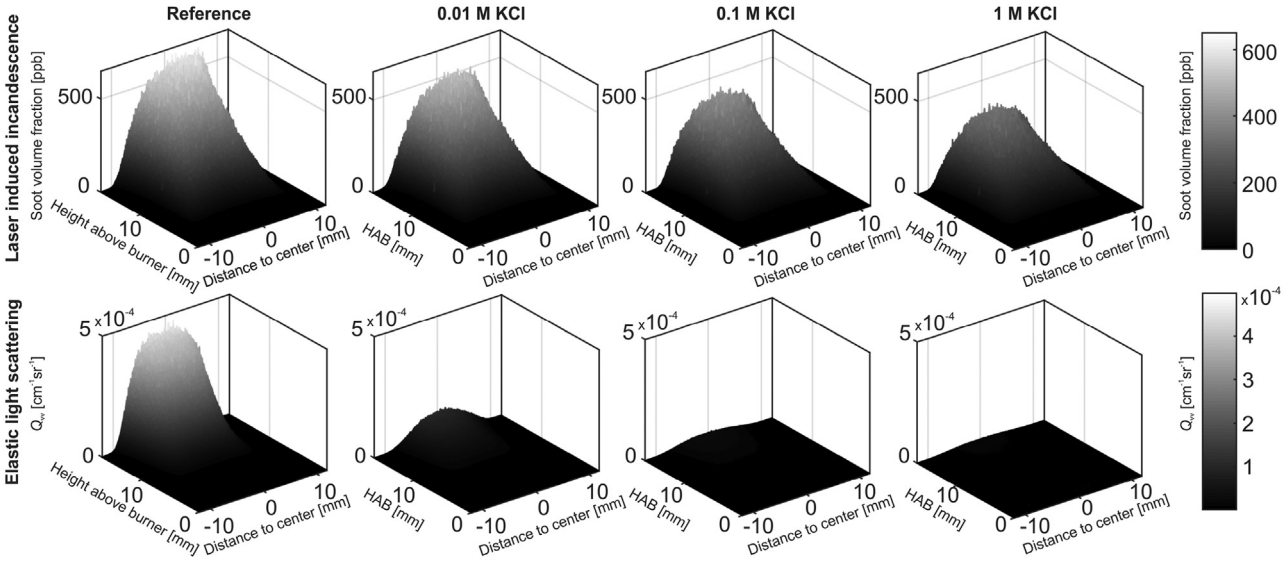

Fig. 2. Soot volume fractions (based on LII measurements) and Q_{vv}-factors (elastic light scattering measurements) as function of height above burner and distance from center in the flame for the reference flame and the flames seeded with 0.01 M, 0.1 M, and 1 M KCl solution.

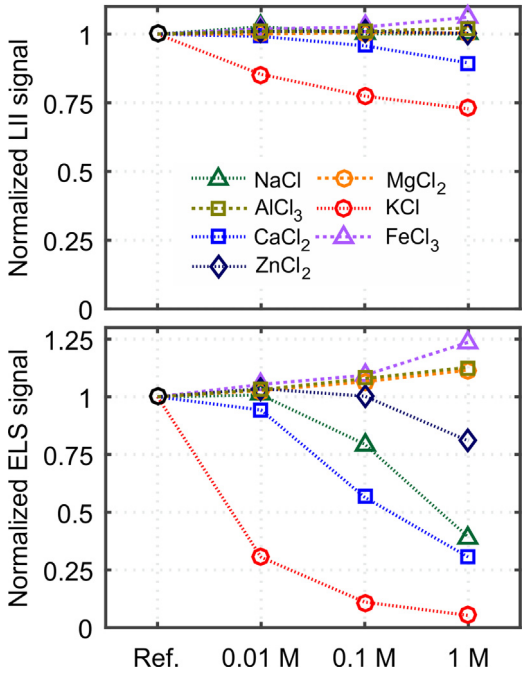

Fig. 3. LII and ELS signals normalized against the reference flame. The data presented has been measured at 10 mm HAB.

concentrations and for the highest concentrations of $CaCl_2$. However, for the ELS measurements we can observe large decreases not only for seeding of KCl and $CaCl_2$, but also for NaCl and $ZnCl_2$. The induced LII signals are, as described in Section 2, proportional to a factor d^3, where d is the soot primary particle diameter. For ELS the power dependence of the particle diameter is d^6, which makes ELS much more sensitive to changes in particle size. The combination of LII and ELS signals has in the present work been used for evaluation of particle sizes, which will be discussed in Section 4.7. The addition of the other salts ($FeCl_3$, $MgCl_2$ and $AlCl_3$) leads at 10 mm HAB to marginal changes in LII signals and slight increase in ELS signals, which will be discussed further in Sections 4.3 and 4.4.

4.3. Axial profiles of LII and ELS for all additives

More details about the influence of the metal chloride additives on soot formation are presented in Fig. 4, where spatially resolved information is shown for all cases. The figure contains 21 graphs separated in rows and columns. All results are presented as function of height above burner (HAB) and are averaged ±2 mm horizontally from the center axis of the flame. Column 1 shows LII measurements presented for the entire measurement region, 1–17 mm HAB. The ELS measurements are shown for the entire measurement region (column 2) as well as more detailed information for the pre-reaction region, the pre-soot region as well as the soot inception region, i.e. 1–8 mm HAB (column 3). The columns are hence described by numbers 1, 2 and 3, and the seven rows are described by letters A to G. The seven rows contain measurement data from the use of different salts in the order from lowest to highest atomic number. The notation is that, for example, Fig. 4(C2) describes the elastic light scattering measurements for aluminum chloride for the entire measurement region.

When observing the LII results in the first column in Fig. 4, a first observation is that all metal salts only have a marginal influence on the soot volume fraction in the soot inception region. At higher HAB, in the soot-growth region, there is a group of metal salts giving only a marginal influence on the soot volume fraction. These are $MgCl_2$, $AlCl_3$, $FeCl_3$, and $ZnCl_2$, with the data presented in Fig. 4(B1, C1, F1, G1). Zinc chloride, however, show a slightly larger effect than the other three, with a decrease in soot volume fraction for the highest salt concentration. Another group, including NaCl, KCl, and $CaCl_2$, gives clearly lower soot volume fractions at higher HAB, these can be seen in Fig. 4(A1, D1, E1). For the latter group, it is also clear that for increasing salt concentration, there is a decrease in the soot volume fraction.

The elastic light scattering results for the entire measurement region are presented in the second column of Fig. 4, and here a logarithmic scale has been used to present the data clearly despite more than three orders of magnitude variation in signal intensity. When adding salt solution to the flame, several additives, including $MgCl_2$, $AlCl_3$, and $FeCl_3$, lead to flames that are marginally influenced (less than ~3%) at the highest heights in the soot-growth region when it comes to the ELS signal. The salts that results in

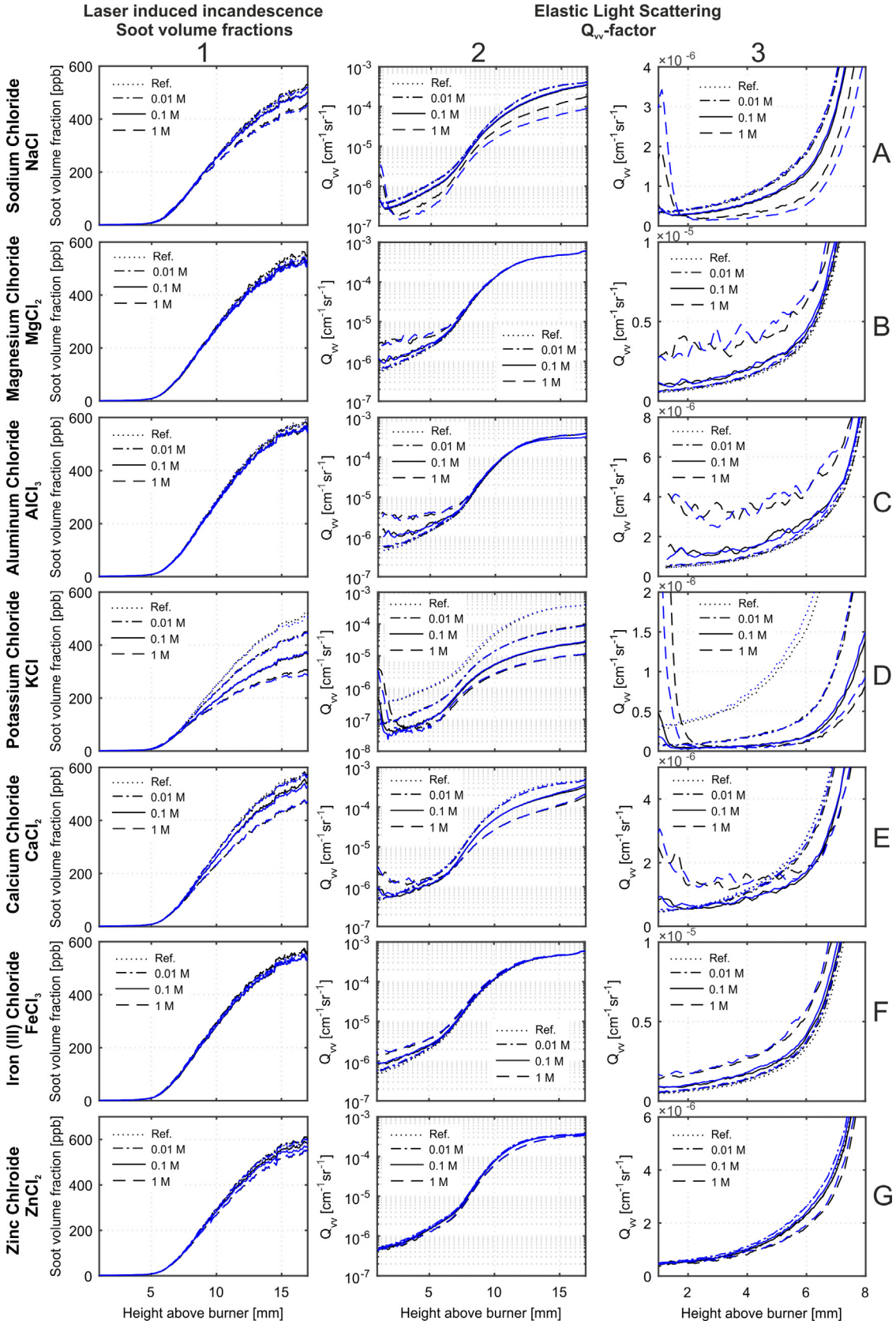

Fig. 4. Soot volume fraction and Q_{vv}-factor as function of height above burner for all measured salts (in order: NaCl, $MgCl_2$, $AlCl_3$, KCl, $CaCl_2$, $FeCl_3$ and $ZnCl_2$). The Q_{vv}-factor is shown for the entire measurement region as well as for a magnified region at low heights above burner. For each flame condition, two intensity profiles from signal averaged data are shown.

most significant change in the soot-growth region are those which also changed the soot volume fraction to a large extent, i.e. NaCl, KCl, and $CaCl_2$, see Fig. 4(A2, D2, E2). A slight decrease for the highest concentration of $ZnCl_2$ could also be observed as shown in Fig. 4(G2).

The third column contains the same information as the initial part of the graphs in the second column, now presented in a linear scale to highlight the differences in the pre-reaction (0–2 mm), the pre-soot (2–4 mm) and the soot inception region (4–8 mm). In the flames investigated, the soot starts to appear with its thermal visible radiation at approximately 4 mm HAB, independent of which salt that was added. For sodium chloride, Fig. 4(A3), we can in the soot inception region, as discussed earlier, see a decrease in ELS signal for increased NaCl concentration. The same effects can be observed in the soot-inception region for potassium chloride, calcium chloride, and the highest concentrations of zinc chloride, Fig. 4(D3, E3, G3). It is also interesting to note that there is a strong decrease in ELS signal, especially for sodium and potassium chloride, compared to the reference flame in the pre-soot region for increased salt concentrations.

Another interesting observation is made close to the burner, in the pre-reaction region, for several of the flames in column 3. As shown in Fig. 4(A3 and D3), both sodium and potassium additives show initially strong scattering which decreases fast from 1 to 2 mm, and also that higher concentrations of these additives give higher initial signal. The increased signal found in the pre-reaction region is most likely due to scattering by the salt particles themselves, as the excess signal disappears for NaCl and KCl when approaching the higher temperatures in the reaction zone located at around 2 mm HAB. This observation can be associated with dissociation of the salt particles. For $MgCl_2$, $AlCl_3$ and $FeCl_3$, shown in Fig. 4(B3, C3, F3), there is also an excess ELS signal, which is larger for higher salt concentrations. This excess scattering seems to persist through the pre-soot region into the soot inception region of the flames, which indicates that the salt particles survive the transport through the high-temperature region in the reaction zone. For the calcium chloride seeded flame, Fig. 4(E3), there seems to be a combined effect of 1) salt particles surviving in the high-temperature region giving an excess scattering signal and 2) a decreased scattering for increased salt concentrations as observed also for additions of sodium and potassium chloride, Fig. 4(A3, D3). A discussion of these observations related to the physical properties of the salts can be found in Section 4.10. Also, the excess scattering phenomenon was further investigated in low-sooting flames, and the results are presented in Section 4.4.

The evaluation of soot volume fractions does come with some uncertainties, especially regarding the absorption function, $E(m)$. First of all, the value of the absorption function of the soot particles varies quite much in the literature, which is a major uncertainty. In [42], a large number of complex refractive indices for soot from various sources and measured using a variety of techniques are presented, and if these are converted to $E(m)$, the values vary between approximately 0.2 to 0.5. This means that there is a quite large uncertainty in evaluated soot volume fraction, as this parameter is inversely proportional to $E(\mathrm{m})$. Secondly, work in our group has showed increasing $E(m)$ with height above burner in similar ethylene/air flames, which means that the soot volume fraction may be under- or overestimated if a constant $E(m)$ is chosen. In this work, $E(m) = 0.35$ was chosen, which is a reasonable value according to [38,39] for HAB larger than 10 mm. The most significant change in $E(m)$ occurs early in the soot growth region (below 9 mm HAB) [38,39]. Selecting an $E(m)$ above this HAB will only give minor uncertainties for most HAB. However, the soot volume fractions at lower HAB will then be underestimated.

4.4. ELS in low-sooting flames

To investigate the effect of the ELS contribution caused by the salt particles further, the flame was adjusted to create a low-sooting flame just above the visible sooting threshold. The flows of this flame were set to 0.21 l/min for ethylene and 1.5 l/min for air, i.e. $\phi = 2.0$. This means a slight decrease in total flow, but as the salt solutions are carried by the air flow, the air flow was kept constant to seed the same amount of salt solution. The co-flow remained at 5 l/min as in all earlier measurements. In Fig. 5, the results of the low-soot measurements are presented for flames seeded with a 1 M solution of NaCl, KCl, $CaCl_2$, $FeCl_3$, and $ZnCl_2$. It should be noted that the reference flame presented in Fig. 5 is a low-sooting flame seeded only with distilled water, hence different from the reference flame discussed in relation to Fig. 4. The ELS signal from the reference flame is shown in all graphs of Fig. 5, where initially the scattering from mainly the combustion gases can be seen up to a height of around 8 mm, after which the scattering strongly increases as a function of height due to scattering from growing soot particles. However, the scattering at the higher heights, around 15 mm, is around three orders of magnitude lower than for the strongly sooting reference flame presented in Figs. 2–4.

The results of Fig. 5 show the same trends as the previously discussed data in Fig. 4. Both sodium and potassium chloride additions lead to less scattering compared to the reference flame at all heights above 2 mm in the low-sooting flame. Another observation is that the excess scattering signal is rather constant throughout the measurement region for the addition of salts of calcium, iron and zinc but with a much lower scattering intensity for zinc. The scattering contributions from the aluminum and magnesium cases are not shown in the figure but have similar appearance as that for the iron (III) chloride case. The observations may be explained as follows. The dissolved salts are aspirated into the air flow as droplets with metal and chloride ions. The droplets evaporate during the transport toward the reaction zone of the flame and metal chloride particles are formed. For sodium and potassium chloride there is an initial decay in the scattering signal as can be seen in Fig. 4(A3, D3), which can be interpreted as dissociation of the sodium and potassium chloride particles. On the other hand, for iron (III) chloride, for instance, the metal chloride particles seem to survive the high temperature reaction zone, since a relatively constant scattering contribution can be observed at all heights in the low-sooting flame of Fig. 5. It can be assumed that the same behavior is valid for the high-sooting flames presented in Fig. 4, i.e. that there is a rather constant scattering contribution from some of the metals at all flame heights, and this is most probably the reason why the ELS signal increases with metal chloride concentration for $MgCl_2$, $AlCl_3$ and $FeCl_3$ in Fig. 3.

4.5. Depolarization ratio in potassium-seeded flames

To primarily ascertain uncertainties in the scattering measurements due to fluorescence and subsequently the particle size evaluation, measurements of the elastic light scattering were performed both for vertical polarization and horizontal polarization for the high-sooting flame. The measurements were conducted when seeding various concentrations of potassium chloride as well as for the reference flame. In Fig. 6 the depolarization ratio, ρ_v, is shown for the entire measurement region of 1 to 17 mm HAB. In our measurements this is the ratio between the scattered intensity of the horizontal polarization, I_{HV}, and the scattered intensity of the vertical polarization, I_{VV}, for vertically polarized incident light, where the first subscript is the polarization of the detected light and the second subscript is the polarization of the incident light [43]. The reference flame has an almost constant depolariza-

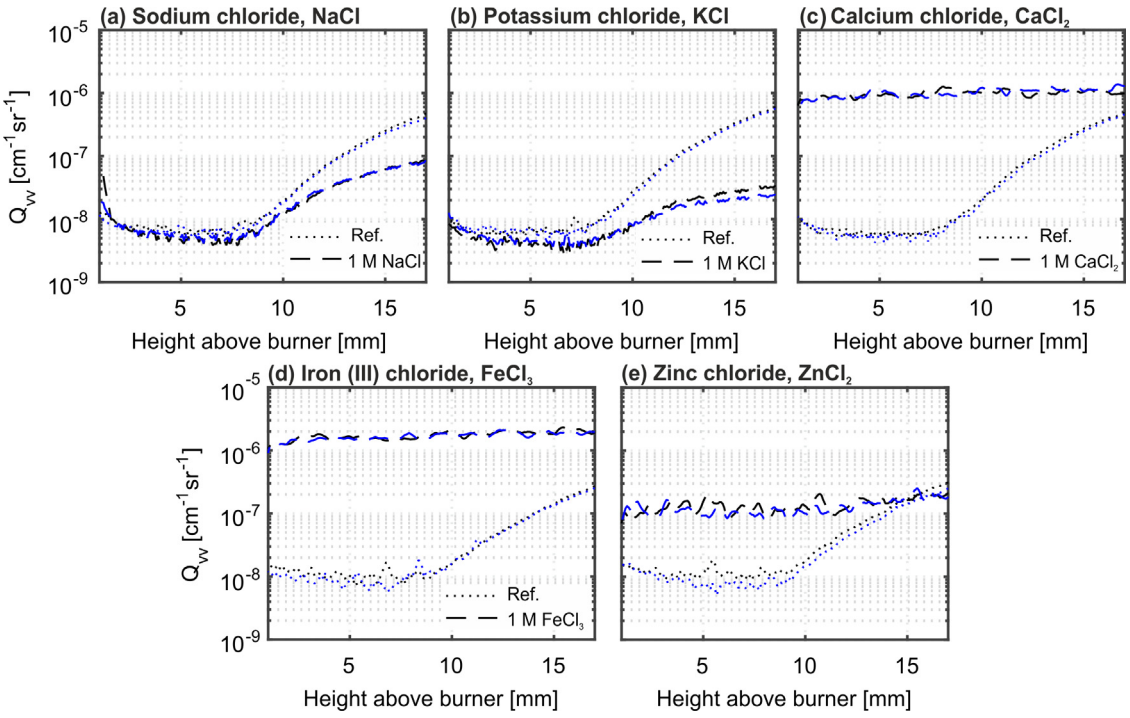

Fig. 5. Q_{vv}-factor as function of height above burner shown for NaCl, KCl, $CaCl_2$, $FeCl_3$ and $ZnCl_2$ for low-sooting conditions to show the effect of scattering from the salt particles themselves for the different types of salts used. The reference flame in this image is the low-sooting reference flame, i.e. low-sooting flame seeded with distilled water.

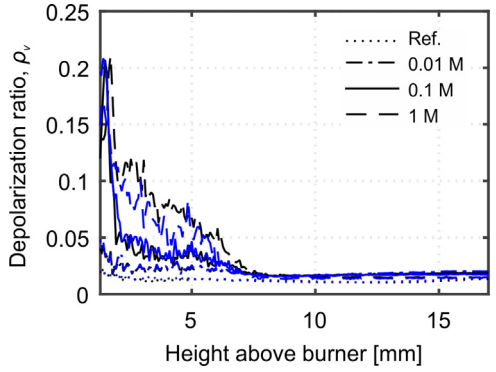

Fig. 6. Depolarization ratio, ρ_v, as function of height above burner for the reference flame and three concentrations of the potassium chloride flame (0.01 M, 0.1 M and 1 M).

tion ratio (0.011 to 0.013) across the measurement region, which is in good agreement with results from a previous study [43]. In the pre-reaction zone (below 2 mm HAB), the depolarization ratio increases for an increased potassium chloride concentration, which may be related to the shape of the salt particles. In the pre-soot and the soot inception region, the depolarization ratio is highest for the largest concentrations of KCl, and gradually decreases for increasing HAB. The origin of this excess depolarization is not clear, but we speculate that there is a fluorescence contribution from polycyclic aromatic hydrocarbons (PAHs), which are well-known to lead to unpolarized fluorescence also for wavelengths in the visible region around 532 nm [44]. We speculate that the increased depolarization ratio is mainly due to that the increased amount of KCl decreases the particle sizes of both the soot precursors and the initial soot particles as discussed in [23], resulting in a decrease in the ELS signal caused by the soot and its precursors, and that the influence of the additives on the PAH concentration and the subsequent fluorescence is smaller. Nevertheless, from Fig. 6, it can be observed that the contribution from potential fluorescence is smaller than 8% for all concentrations and heights in and above the soot inception region. In the soot growth region, the depolarization ratio for the flames seeded with potassium chloride show minor variations as a function of height above burner. These variations for the various concentrations of KCl and the reference flame in the soot-growth region could be related to the PAHs fluorescence as discussed but may also at least partly originate from a change of the morphology and size of particles as discussed by Sorensen in [43]. Accordingly, we can conclude that the interference of fluorescence to the scattering is below 8% in the soot inception region (4–8 mm), and less than 2% in the soot growth region (8–17 mm).

4.6. Particle sizing using TEM

In Fig. 7, typical soot aggregates are shown, studied using transmission electron microscopy (TEM) for the reference flame and some selected flames seeded with the highest, 1 M, concentration. The TEM analysis were performed on soot sampled at 10 mm HAB. Based on measurements of primary particle diameters in aggregates in the TEM images, statistical information for each of these salts has been evaluated and can be found below each image. The results from the TEM evaluation show that there is a significant decrease in primary particle size when adding potassium chloride and a slight decrease for calcium chloride additives. However, for NaCl the difference from the reference flame is minor. These results are in agreement with Bonczyk et al. [16], where they investigated particle sizes based on extinction and elastic light scattering measurements and found a significant decrease for potassium additives but only minor changes for calcium and sodium, as was also observed in the present work. Further evaluation of particle sizes using LII and ELS were performed for the reference flame and the potassium seeded flame, as there was an effect on particle size seen in the TEM images reported here and in our previous paper [23]. A discussion regarding the uncertainties for the evaluated

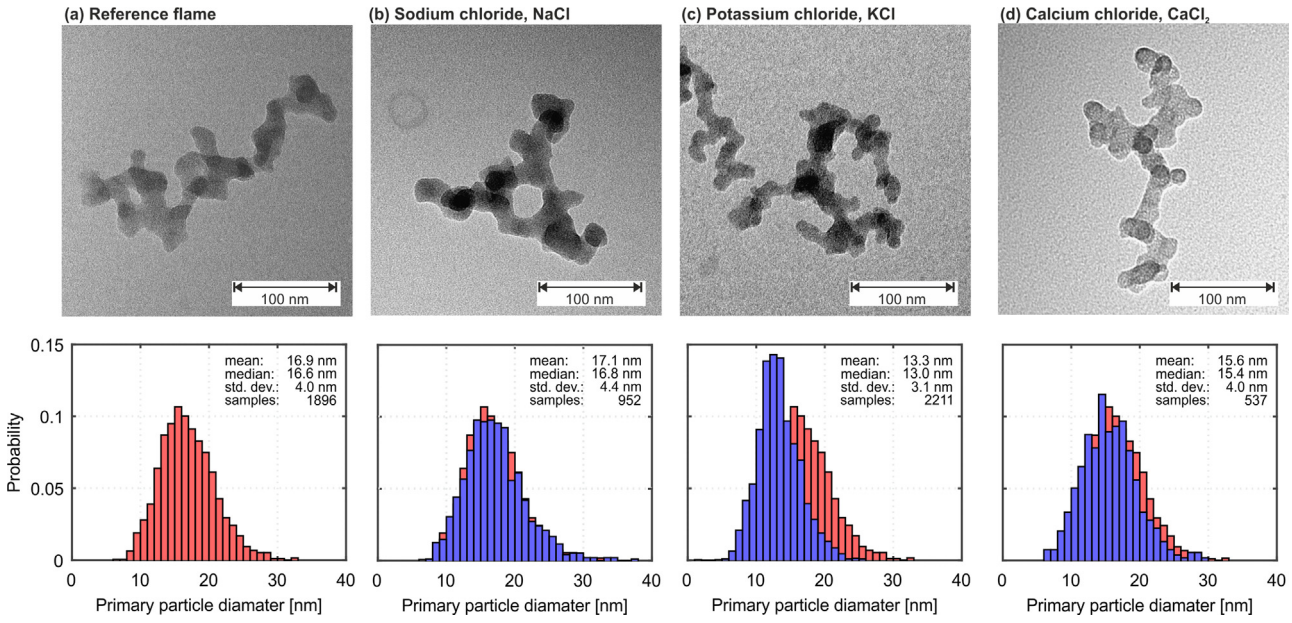

Fig. 7. Images of soot aggregates and statistical information of primary particle sizes based on TEM measurement for (a) the reference flame, (b) the sodium chloride seeded flame, (c) the potassium chloride seeded flame, and (d) the calcium chloride seeded flame. The histogram shown in Fig. 7a has been included in the background of each of the other figures to simplify comparison.

particle sizes from both TEM and LII/ELS can be found at the end of Section 4.7.

4.7. Particle sizing axially using combined LII and ELS

By using the LII signals calibrated to soot volume fractions and the elastic light scattering measurements presented in Fig. 4, soot particle sizes could be evaluated using the theory presented in Section 2. In Fig. 8 primary particle sizes are shown from evaluations initially by assuming that there is no aggregation (Fig. 8a), and by taking aggregation into account (Fig. 8b). For the evaluation of primary particle sizes in this work, $E(m) = 0.35$ has been used for all HAB, and $F(m)$ was calculated to be 0.217 based on a refractive index used by Reimann et al. in [36].

In Fig. 8a, primary particle sizes are displayed from evaluations without taking aggregation into account. Combining Eqs. (2) and (4) results in the following expression for the soot primary particle diameter, d:

$$d = \sqrt[3]{\frac{Q_{vv}}{f_v}\frac{2\lambda^4}{3\pi^3}\frac{1}{F(m)}} = \sqrt[3]{\frac{Q_{vv}}{K_{ext}}\frac{4\lambda^3}{\pi^2}\frac{E(m)}{F(m)}} \tag{8}$$

The particle sizes in Fig. 8 are presented for the reference flame, and three concentrations of potassium chloride, mainly for the soot-growth region (6 to 17 mm HAB), where the influence of PAH fluorescence interference to the ELS signal is negligible. The results show that particle sizes increase with HAB as expected, however the sizes presented are significantly higher than those observed based on the TEM evaluation. It should be noted that soot samples for the TEM evaluation have only been taken at 10 mm HAB. It is clear from the images shown in Fig. 7 that the particles are aggregated, hence this effect should be taken into account.

In Fig. 8b, evaluation of the primary particle sizes has been performed using Eqs. (5) and (6), resulting in an expression for the particle diameter taking aggregation into account:

$$d = \sqrt[3]{\frac{Q_{vv}}{f_v}\frac{2\lambda^4}{3\pi^3}\frac{1}{F(m)}\frac{1}{n}\frac{1}{S(q)}} = \sqrt[3]{\frac{Q_{vv}}{K_{ext}}\frac{4\lambda^3}{\pi^2}\frac{E(m)}{F(m)}\frac{1}{n}\frac{1}{S(q)}} \tag{9}$$

For the evaluation performed in Fig. 8b, the structure factor, $S(q)$ was set to 1, assuming to be within the Rayleigh regime. The

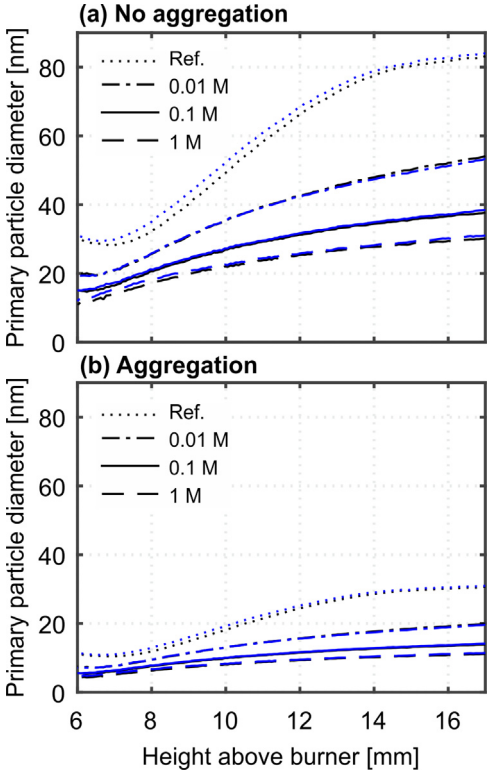

Fig. 8. Evaluated primary particle sizes as function of height above burner from 6 to 17 mm assuming no aggregation in (a) and by taking the aggregation into account in (b). Both graphs show data from the reference flame along with the three concentrations of KCl (0.01 M, 0.1 M and 1 M) seeded into the flame.

number of primary particles per aggregate, n, was estimated to 20, for both the reference flame and the potassium chloride seeded flame based on TEM analysis at 10 mm HAB. The same value was used for both cases as reliable statistics for the number of particles per aggregate is hard to estimate from TEM images. Also the value

chosen of n is not representative for all HABs, as less and more aggregation is expected for lower and higher HAB, respectively. The results shown at 10 mm HAB in Fig. 8b are in fair agreement with the results of the TEM analysis of soot sampled at 10 mm HAB. For soot in the reference flame, the difference is minor, as the TEM analysis results in an average primary particle size of 16.9 nm, while the evaluated particle sizes from optical measurements are 18.6 nm. For the potassium-seeded flame, the soot particle size averaged from TEM showed a particle size of 13.3 nm, while the combined LII and ELS data resulted in 8.2 nm. Hence, for this case the discrepancy is larger, but the results show the expected trend.

We can also note from the LII and ELS measurements presented in Figs. 3 and 4 that additives of NaCl, $CaCl_2$ and $ZnCl_2$ decrease the ELS signal relatively more than the decrease measured in soot volume fraction. Since ELS is much more sensitive to changes in primary particle diameter than LII, it is reasonable to assume that this indicate smaller particles.

In the analysis of sizes from the combined LII/ELS data we estimate that the experimental uncertainties are much smaller than those arising from uncertainties in the theoretical description. For example, in the soot growth region the influence of fluorescence to the scattering was shown to be below 2 %, see Section 4.5. In the theoretical evaluation large uncertainties arise from the optical parameters $E(m)$ and $F(m)$ as well as the number of particles per aggregate and the factor $S(q)$ which was set to one. The uncertainties related to the absorption function, $E(m)$, was discussed in Section 4.3. If we do the same analysis for $F(m)$, which also is derived directly from the complex refractive index of soot, we can for the refractive indices presented in [42] see a variation from 0.2 to 0.7. The primary particle diameters evaluated using LII and ELS are proportional to the cube root of the ratio between $E(m)$ and $F(m)$. Using the evaluated $E(m)$ and $F(m)$ in pairs from [42] and comparing with the values used in the present evaluation results in uncertainties of 20–30% in the particle size evaluation.

The uncertainties of the structure factor, $S(q)$, are harder to estimate. By setting the structure factor to one, we will most likely underestimate the primary particle size, as $S(q)$ always is smaller or equal to one according to Eq. (7). In work by Reimann et al. [36], a comprehensive analysis of primary particle sizes evaluated using LII and ELS has been performed on soot from a premixed ethylene/air flame ($\phi = 2.7$) on a McKenna burner. If we assume qR_g to be approximately one, resulting in $S(q) = 0.67$, which is comparable with the results presented in [36], an estimation of the error is possible. Primary particle sizes are inversely proportional to the cube root of $S(q)$ which means that the primary particle sizes may be underestimated by up to 14%. Furthermore, the average number of particles per aggregate is hard to estimate for several reasons: (1) the uncertainties in how well the sampled soot particles are representative of the in situ flame soot particles, and (2) there is in reality an aggregate distribution and it requires analysis of a very large number of aggregates to certify this. Moreover, manual evaluation of particle sizes from TEM is both time consuming and subjective as the evaluator has to determine by hand the location of boundaries for each primary soot particle, which also introduces some uncertainty in the size evaluation. These uncertainties are hard to estimate, but repetitive evaluation of the same data material resulted in uncertainties of a few percent. An automated evaluation approach would be faster and estimation of the error would probably be easier, but the method might not be more accurate. Overall, we can conclude that evaluating particle sizes comes with large uncertainties, but the evaluation still gives reasonable numbers compared to TEM evaluated samples, and do give good indication of the changes that occurs when adding various salts to the flame.

4.8. Particle sizing radially using combined LII and ELS

So far, the evaluations have dealt with the premixed flames and changes versus height above burner. The use of two-dimensional detection both for ELS and LII enabled simultaneous studies of the effects of additives at the flame edges where the products from the fuel-rich flame burn as a diffusion flame. In Fig. 9, normalized LII and ELS signals are shown as well as evaluated primary particle diameters radially for the flame at 10 mm height above burner. Several of the salts ($MgCl_2$, $AlCl_3$, $FeCl_3$, and $ZnCl_2$) showed marginal effect at the edges, and we have chosen to present data for the two salts ($CaCl_2$ and KCl) that gave the strongest impact on the sooting behavior. In Fig. 9(a) and (b), all LII and ELS data have been normalized at flame center, and for comparison between the real values at this point, see Fig. 4. At first we note that the LII signal, and thereby the soot volume fraction, decreases toward the edges for the reference flame because of oxidation. For additions of $CaCl_2$ and KCl, the normalized LII signal only show marginal decrease compared to the reference flame at the edges. However, for the ELS measurements, there is a decrease of signal toward the edges for the reference flame, but here both $CaCl_2$ and KCl additives lead to a relatively stronger decrease.

Evaluation of particle sizes were also performed for $CaCl_2$ and KCl additions for the cross section at 10 mm HAB. For the particle size evaluation, Eq. (9) was utilized, assuming an average of 20 particles per aggregate for both the reference and the flames seeded with $CaCl_2$ and KCl. The results in Fig. 9c and d clearly show a decrease in primary particle sizes toward the edge for the reference flame, which is expected as more oxidation occurs in this area. In comparison with the reference flame, the LII and ELS results indicate also a stronger relative size reduction at the flame edge in comparison with the flame center for the additions of 1 M $CaCl_2$ and 1 M KCl. For $CaCl_2$ the relative decrease in particle size was 41% at the flame edge (~7 mm from center) in comparison with 29% at the center, while the corresponding values for KCl were 65% in comparison with 56%. Hence, in both flames there is increased soot oxidation at the edges as a result of both additives.

Another observation in Fig. 9c and d is that the effect to the particle sizes by adding potassium to the flames is clearly larger than when adding calcium based on the evaluation of the combined ELS and LII data. These data thus support the trend that was observed in the TEM image analysis in Fig. 7. It should be noted that the observation of a scattering contribution from $CaCl_2$ in the low-sooting flame can be expected also in the here discussed flame, and if it has the same magnitude this contribution to the ELS signal is on the order of 5% of the ELS signal from the soot.

4.9. Influence of potassium on flame temperature

In the present work it has been observed that for flames with potassium seeding, the soot volume fraction remains relatively unaffected in the soot inception region (4–8 mm) and becomes lower in the soot growth region (8–17 mm), see Fig. 4. It is well-known that potassium has the effect of reducing soot concentration and particle size [12,16], but it is also important to observe if other flame parameters change as a result of the potassium addition. A critical parameter is the temperature. Harris and Weiner performed measurements in premixed laminar ethylene/air-flames [45,46] and observed that increased temperatures resulted in lower soot volume fractions. Hence, it is highly relevant to identify if there are temperature differences in the flames with and without potassium seeding.

In Fig. 10, temperature profiles are shown from the flames studied in the present work, with and without seeding of potassium. The results have been measured using rotational coherent

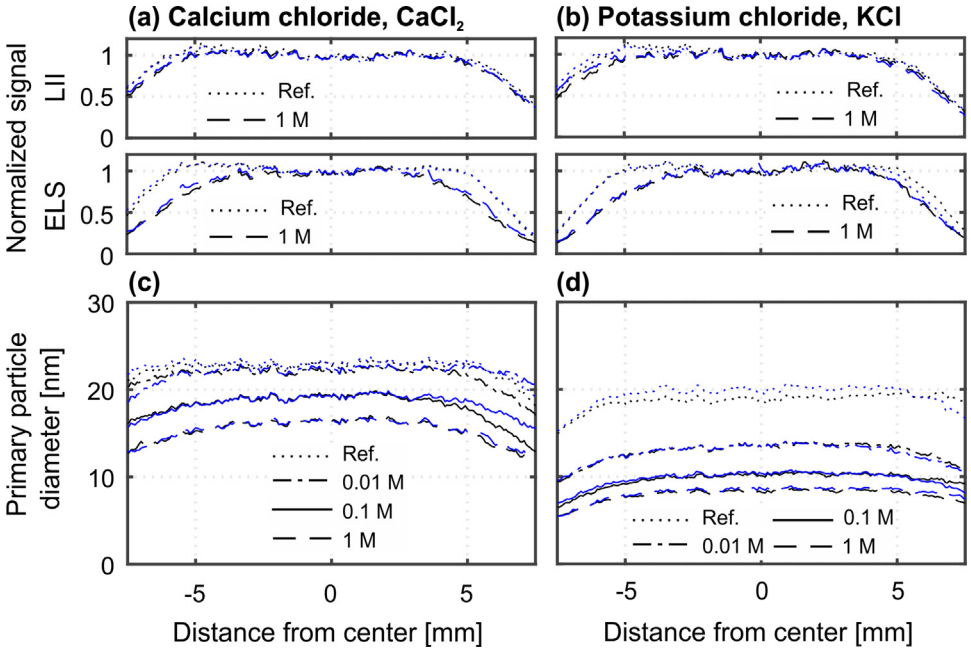

Fig. 9. Investigation of edge effects for potassium and calcium chloride at 10 mm HAB. In (a) and (b) normalized LII and ELS signals are shown for the reference flame and the highest concentration of calcium and potassium chloride respectively. In (c) and (d) evaluated primary particle sizes are shown for the reference flame and all concentrations of salts for $CaCl_2$ and KCl. The edges of the flame are located at approximately ±8 mm from center, i.e., just outside the region showed.

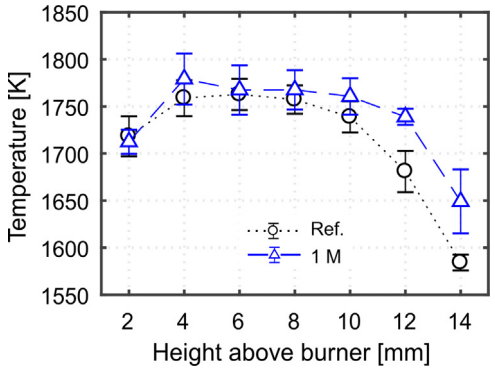

Fig. 10. Flame temperature profiles measured using rotational CARS thermometry for the reference flame and the 1 M potassium chloride-seeded flame.

anti-Stokes Raman spectroscopy [47,48] at the central axis. The setup utilised a planar dual broadband BOXCARS approach and an LDS dye with a center wavelength of around 690 nm. Temperatures were evaluated from nitrogen, which had line intensities of more than two orders of magnitude more than spectral contributions of CO and CO_2. For improved temperature accuracy, line-broadening from H_2O, and H_2 were included in the calculation of the spectral libraries used for fitting of the temperatures [47].

The results of Fig. 10 show that the flame temperature is higher for the potassium-seeded flame with an average temperature difference of 30 K. In more detail, the first observation is that the evaluated temperature in the early soot inception region (4–8 mm) is slightly higher for the flame with potassium addition in comparison with the reference flame. The difference temperature is very small, only 10–15 K. This is slightly higher than the assumed uncertainty limit of the CARS technique, and hence there is an indication of a higher temperature for the case with potassium addition. The reason for this difference is not clear. When discussing this small temperature difference above, the accuracy of the CARS technique for thermometry should be discussed. In general the uncertainty for the CARS technique is estimated to 2–3%. However, for a measurement series such as the present one, we have continuously changed between the two conditions (with and without seeding) within the same measurement series. By using such a strategy, the systematic errors are cancelled in the evaluation of the temperature difference. We estimate that we can be observe differences that are higher than 10 K by this approach, and thereby that the flame temperature with potassium seeding is slightly higher in the whole sooting region from the inception region and through the soot growth region.

The second observation in Fig. 10 is that the temperature difference between the two flames increases as a function of HAB from 8 to 14 mm. In this range the soot volume fraction increases faster with height in the non-seeded flame. Consequently this non-seeded flame will suffer from stronger radiation loss than the seeded one, which leads to a larger difference in temperature between the two curves. Since, according to Harris and Weiner [45,46], an increased temperature in ethylene/air flames leads to lower soot concentration, the present observation of lower soot concentrations in the potassium-seeded flames may partly be due to a temperature effect.

4.10. Properties of the metal atoms and salts

We have in this paper shown that some metal salts can significantly impact soot formation, more specifically the salts containing either alkali or alkaline earth metals, in our case potassium, sodium, and calcium. What is the reason that these metals are affecting the soot concentration in this way? A common observation is that the influence correlates well with the ionization potential of the metal. Bonczyk performed a detailed study in which five alkali metals (Li, Na, K, Rb, and Cs) were injected to premixed flames [16]. Through scattering/extinction measurements, soot particle sizes and volume fractions were deduced. It was shown that the volume fraction weakly decreased and evaluated size strongly decreased with increasing atomic number of the alkali atom, which in turn correlates with lower ionization potential. The review paper by Howard and Kausch [14] and references therein also discussed

Table 1
Some characteristics of metal atoms used in the present investigation. The table includes the atomic number, ionization potential, as well as lattice energies for their chlorides. The lattice energies have been estimated based on the Born–Haber cycle described in [49] using data from [50–52].

Metal	Atomic number (group)	Ionization potential [50](first electron)	Lattice energy per salt molecule
Sodium (Na)	11 (alkali metal)	5.14 eV	8.16 eV
Magnesium (Mg)	12 (alkaline earth)	7.65 eV	26.1 eV
Aluminum (Al)	13 (basic metal)	5.99 eV	56.9 eV
Potassium (K)	19 (alkali metal)	4.34 eV	7.43 eV
Calcium (Ca)	20 (alkaline earth)	6.11 eV	23.5 eV
Iron (Fe)	26 (transitional metal)	7.90 eV	56.1 eV
Zinc (Zn)	30 (transitional metal)	9.39 eV	28.3 eV

that the alkali metals ionize the flames significantly due to their low ionization potential, which leads to lower coagulation rates for soot. In Table 1, the ionization potentials are shown for the here analyzed metal additives.

In the present investigation, many of the metal atoms were observed to not interact with the flame and seemed to pass the flame giving strong scattering contribution. We interpret this excess scattering as that the metal and chloride ions, which were dissolved in the water and aspirated into the flame, recombine and form metal chloride particles. Hence, for these metals that are bound in salts the ionization potentials have no importance. Instead it is of interest to study the lattice energies, i.e. the energy it takes for a molecule to break apart from a solid salt crystal to ions in gas phase, for the metal salts in this investigation. The lattice energies, shown in Table 1, have been calculated using the Born–Haber cycle [49], which primarily work for alkali halides. However, in an effort to compare the lattice energies we have used it for all salts.

From Table 1 it is shown that potassium and sodium chloride have low lattice energies (~8 eV), which explains why they dissociate when they pass through the reaction zone. Together with the low ionization potential of potassium and sodium, this could explain why additives of KCl and NaCl are so effective in reducing the amount of soot. Two other salts that also reduce the soot formation are $CaCl_2$ and $ZnCl_2$, which both have calculated lattice energies in the mid-range (~25 eV). Calcium has fairly low ionization potential, which could explain why this is more effective than both zinc and magnesium. However, as discussed by Howard and Kausch [14], ionization may not be the main reason why calcium reduces the amount of soot, instead the additives together with the flame gases are suggested to create hydroxyl radicals which lowers the amount of soot and precursors of soot.

Aluminum chloride and iron chloride both have very high lattice energies (~56 eV) which could explain why these do not show any effect in reducing the amount of soot, and why they result in excess scattering throughout the sooting region of the flame. To conclude this part, it seems reasonable that the effect of metal additives is strongly related to the method by which the metals are introduced to the flame as well as its chemical properties, and the flame conditions.

5. Conclusions

In this work, we have demonstrated the use of combined laser-induced incandescence (LII) and elastic light scattering (ELS) for retrieving information about soot properties in sooting flames and valuable information about the influence of various salts and salt concentrations on these properties. Seven different metal salts (NaCl, $MgCl_2$, $AlCl_3$, KCl, $CaCl_2$, $FeCl_3$, and $ZnCl_2$) were dissolved in water and seeded into premixed ethylene/air flames through the oxidizer (air).

The main conclusions from this paper are:

- Optical diagnostics using combined LII and ELS has been successfully used for retrieving two-dimensional data on both soot volume fraction and sizes.
- Although the metal chlorides were dissolved in water before entering the flame, three salts ($MgCl_2$, $AlCl_3$, and $FeCl_3$) seemed to pass the flame without clear interaction with the flame, which was manifested through a scattering contribution related to salt particles. Two of the salts ($CaCl_2$, $ZnCl_2$) showed signs of partial dissociation and influenced soot formation in the flames to some extent. The alkali salts (NaCl, KCl) seemed to be fully dissociated and did not show any effect of scattering contribution after passing through the reaction zone of the flame.
- In the soot inception region only marginal effect on the soot volume fraction was observed, independent on which salt was aspirated into the flame. The scattering measurements, however, showed a significant signal decrease when adding potassium and sodium chloride, indicating smaller soot particles. We also note that calcium chloride has this behavior, but the effect is hidden due to scattering from the calcium chloride particles themselves.
- Potassium chloride addition had the largest impact on soot formation with some reduction of LII signal (and thereby soot volume fraction) and drastic decrease in ELS signal. Evaluated particle sizes from the combined LII and ELS measurements showed decreasing primary particle sizes with increasing salt concentration. Evaluated sizes are in reasonable agreement with TEM evaluated samples if aggregation is taken into account using the RDG theory for ELS. However, the evaluated size differences between the reference flame and the potassium chloride-seeded flame is larger for the optical measurements compared to the TEM evaluated data.
- Also the calcium chloride-seeded flames showed smaller evaluated particle sizes in the TEM image as well as in the analysis of the LII and ELS measurements. However, TEM evaluated samples do only show marginal size differences for the sodium chloride-seeded flames in comparison with the reference flame, even though the measurements conducted by ELS and LII indicate smaller particles for the seeding with sodium chloride.
- Oxidation effects were studied in the outer diffusion flame of the premixed flames. Both unseeded and flames seeded with potassium and calcium showed clearly smaller particle sizes at the edge in comparison with at the center. For potassium and calcium additives increased oxidation was observed at the edges.
- The flame temperature measured by CARS spectroscopy was higher in the potassium-seeded flame in the soot inception region as well as in the soot growth region with an average difference of ~30 K.

Acknowledgments

The authors would like to thank the Swedish Energy Agency through the Swedish Gasification Centre (SFC) and Bio4Gasification

for their financial support. Henrik Bladh is acknowledged for initial discussions of the work and a broad literature study of the field of metal additives. We thank Peter Glarborg, Technical University of Denmark, for fruitful discussions about potassium chemistry in flames. We would also like to acknowledge Lina Gefors from Lund University Bioimaging Center, Sweden for valuable help during the evaluation of our TEM samples.

References

[1] WHO, Health Aspects of Air Pollution with Particulate Matter, Ozone and Nitrogen Dioxide, Bonn, Germany, 2003 Report No. EUR/03/5042688.
[2] T.C. Bond, S.J. Doherty, D.W. Fahey, P.M. Forster, T. Berntsen, B.J. DeAngelo, M.G. Flanner, S. Ghan, B. Kärcher, D. Koch, S. Kinne, Y. Kondo, P.K. Quinn, M.C. Sarofim, M.G. Schultz, M. Schulz, C. Venkataraman, H. Zhang, S. Zhang, N. Bellouin, S.K. Guttikunda, P.K. Hopke, M.Z. Jacobson, J.W. Kaiser, Z. Klimont, U. Lohmann, J.P. Schwarz, D. Shindell, T. Storelvmo, S.G. Warren, C.S. Zender, Bounding the role of black carbon in the climate system: a scientific assessment, J. Geophys. Res. Atmos. 118 (2013) 5380–5552.
[3] IPCC, Summary for Policymakers, in: T.F. Stocker, D. Qin, G.-K. Plattner, M. Tignor, S.K. Allen, J. Boschung, A. Nauels, Y. Xia, V. Bex, P.M. Midgley (Eds.), Climate change 2013: the physical science basis. Contribution of working group I to the fifth assessment report of the intergovernmental panel on climate change, Cambridge University Press, Cambridge, United Kingdom and New York, NY, USA, 2013.
[4] H. Wiinikka, F. Weiland, E. Pettersson, O. Öhrman, P. Carlsson, J. Stjernberg, Characterisation of submicron particles produced during oxygen blown entrained flow gasification of biomass, Combust. Flame 161 (2014) 1923–1934.
[5] J. Simonsson, H. Bladh, M. Gullberg, E. Pettersson, A. Sepman, Y. Ögren, H. Wiinikka, P.-E. Bengtsson, Soot concentrations in an atmospheric entrained flow gasifier with variations in fuel and burner configuration studied using diode-laser extinction measurements, Energy Fuels 30 (2016) 2174–2186.
[6] E. Bartholomé, H. Sachsee, Katalytische Erscheinungen an Aerosolen, Z. Electrochem. 53 (1949) 326–331.
[7] B. Toone, A review of aero engine smoke emission, Combustion in advanced gas turbine systems, 1967, pp. 271–293.
[8] D.W. Golothan, Diesel engine exhaust smoke: the influence of fuel properties and the effects of using barium-containing fuel additive, SAE International, 1967.
[9] D.H. Cotton, N.J. Friswell, D.R. Jenkins, The suppression of soot emission from flames by metal additives, Combust. Flame 17 (1971) 87–98.
[10] K.C. Salooja, Combustion control by novel catalytic means, Nature 240 (1972) 350–351.
[11] E.M. Bulewicz, D.G. Evans, P.J. Padley, Effect of metallic additives on soot formation processes in flames, Symp. (Int.) Combust. 15 (1975) 1461–1470.
[12] B.S. Haynes, H. Jander, H.G. Wagner, The effect of metal additives on the formation of soot in premixed flames, Symp. (Int.) Combust. 17 (1979) 1365–1374.
[13] B.S. Haynes, H. Jander, H. Mätzing, H.G.G. Wagner, The influence of various metals on carbon formation in premixed flames, Combust. Flame 40 (1981) 101–103.
[14] J.B. Howard, W.J. Kausch Jr., Soot control by fuel additives, Prog. Energy Combust. 6 (1980) 263–276.
[15] P.A. Bonczyk, In-situ optical measurement of additive effects on particulates in a sooting diffusion flame, Combust. Flame 51 (1983) 219–229.
[16] P.A. Bonczyk, Effects of metal additives on soot precursors and particulates in a $C_2H_4/O_2/N_2$/Ar premixed flame, Fuel 70 (1991) 1403–1411.
[17] P.A. Bonczyk, The influence of alkaline-earth additives on soot and hydroxyl radicals in diffusion flames, Combust. Flame 67 (1987) 179–184.
[18] K.E. Ritrievi, J.P. Longwell, A.F. Sarofim, The effects of ferrocene addition on soot particle inception and growth in premixed ethylene flames, Combust. Flame 70 (1987) 17–31.
[19] C. Wong, Characterization of metal-soot systems by transmission electron microscopy, Carbon 26 (1988) 723–734.
[20] D.W. Hahn, T.T. Charalampopoulos, The role of iron additives in sooting premixed flames, Symp. (Int.) Combust. 24 (1992) 1007–1014.
[21] T.T. Charalampopoulos, D.W. Hahn, H. Chang, Role of metal additives in light scattering from flame particulates, Appl. Opt. 31 (1992) 6519–6528.
[22] A.S. Feitelberg, J.P. Longwell, A.F. Sarofim, Metal enhanced soot and PAH formation, Combust. Flame 92 (1993) 241–253.
[23] J. Simonsson, N.-E. Olofsson, H. Bladh, M. Sanati, P.-E. Bengtsson, Influence of potassium and iron chloride on the early stages of soot formation studied using imaging LII/ELS and TEM techniques, Proc. Combust. Inst. 36 (2017) 853–860.
[24] C. Schulz, B.F. Kock, M. Hofmann, H. Michelsen, S. Will, B. Bougie, R. Suntz, G. Smallwood, Laser-induced incandescence: recent trends and current questions, Appl. Phys. B 83 (2006) 333–354.
[25] H.A. Michelsen, C. Schulz, G.J. Smallwood, S. Will, Laser-induced incandescence: particulate diagnostics for combustion, atmospheric, and industrial applications, Prog. Energy Combust. 51 (2015) 2–48.
[26] H. Bladh, J. Johnsson, P.-E. Bengtsson, On the dependence of the laser-induced incandescence (LII) signal on soot volume fraction for variations in particle size, Appl. Phys. B 90 (2008) 109–125.
[27] D.R. Snelling, F.S. Liu, G.J. Smallwood, Ö.L. Gülder, Determination of the soot absorption function and thermal accommodation coefficient using low-fluence LII in a laminar coflow ethylene diffusion flame, Combust. Flame 136 (2004) 180–190.
[28] T. Mouton, X. Mercier, M. Wartel, N. Lamoureux, P. Desgroux, Laser-induced incandescence technique to identify soot nucleation and very small particles in low-pressure methane flames, Appl. Phys. B 112 (2013) 369–379.
[29] H. Bladh, N.-E. Olofsson, T. Mouton, J. Simonsson, X. Mercier, A. Faccinetto, P.-E. Bengtsson, P. Desgroux, Probing the smallest soot particles in low-sooting premixed flames using laser-induced incandescence, Proc. Combust. Inst 35 (2015) 1843–1850.
[30] C.F. Bohren, D.R. Huffman, Absorption and scattering of light by small particles, Wiley, New York, 1998.
[31] C.M. Sorensen, Light scattering by fractal aggregates: a review, Aerosol Sci. Technol. 35 (2001) 648–687.
[32] A. Karlsson, T. Yi, P.-E. Bengtsson, Absorption and scattering of light from ensembles of randomly oriented aggregates, Opt. Soc. Am. A 30 (2013) 316–324.
[33] F. Liu, G.J. Smallwood, Effect of aggregation on the absorption cross-section of fractal soot aggregates and its impact on LII modelling, J. Quant. Spectrosc. Radiat. Transf. 111 (2010) 302–308.
[34] T.T. Charalampopoulos, J.D. Felske, Refractive indices of soot particles deduced from in-situ laser light scattering measurements, Combust. Flame 68 (1987) 283–294.
[35] N.-E. Olofsson, H. Bladh, A. Bohlin, J. Johnsson, P.-E. Bengtsson, Are sooting premixed porous-plug burner flames one-dimensional? A laser-based experimental investigation, Combust. Sci. Technol. 185 (2013) 293–309.
[36] J. Reimann, S.A. Kuhlmann, S. Will, 2D aggregate sizing by combining laser-induced incandescence (LII) and elastic light scattering (ELS), Appl. Phys. B 96 (2009) 583–592.
[37] J. Simonsson, N.-E. Olofsson, S. Török, P.-E. Bengtsson, H. Bladh, Wavelength dependence of extinction in sooting flat premixed flames in the visible and near-infrared regimes, Appl. Phys. B 119 (2015) 657–667.
[38] N.-E. Olofsson, J. Simonsson, S. Török, H. Bladh, P.-E. Bengtsson, Evolution of properties for aging soot in premixed flat flames studied by laser-induced incandescence and elastic light scattering, Appl. Phys. B 119 (2015) 669–683.
[39] H. Bladh, J. Johnsson, N.-E. Olofsson, A. Bohlin, P.-E. Bengtsson, Optical soot characterization using two-color laser-induced incandescence (2C-LII) in the soot growth region of a premixed flat flame, Proc. Combust. Inst. 33 (2011) 641–648.
[40] J.A. Sutton, J.F. Driscoll, Rayleigh scattering cross sections of combustion species at 266, 355, and 532 nm for thermometry applications, Opt. Lett. 29 (2004) 2620–2622.
[41] T. Leffler, Development and application of optical diagnostics of alkali vapours for solid fuel combustion, Department of Physics, Faculty of Engineering, Lund University, Lund, Sweden, 2016.
[42] T.C. Bond, R.W. Bergstrom, Light absorption by carbonaceous particles: an investigative review, Aerosol Sci. Technol. 40 (2006) 27–67.
[43] N. Lu, C.M. Sorensen, Depolarized light scattering from fractal soot aggregates, Phys. Rev. E 50 (1994) 3109–3115.
[44] S. Bejaoui, X. Mercier, P. Desgroux, E. Therssen, Laser induced fluorescence spectroscopy of aromatic species produced in atmospheric sooting flames using UV and visible excitation wavelengths, Combust. Flame 161 (2014) 2479–2491.
[45] S.J. Harris, A.M. Weiner, Surface growth of soot particles in premixed ethylene/air flames, Combust. Sci. Technol. 31 (1983) 155–167.
[46] S.J. Harris, A.M. Weiner, Some constraints on soot particle inception in premixed ethylene flames, Symp. (Int.) Combust. 20 (1985) 969–978.
[47] F. Vestin, M. Afzelius, C. Brackmann, P.E. Bengtsson, Dual-broadband rotational CARS thermometry in the product gas of hydrocarbon flames, Proc. Combust. Inst. 30 (2005) 1673–1680.
[48] S. Roy, J.R. Gord, A.K. Patnaik, Recent advances in coherent anti-Stokes Raman scattering spectroscopy: fundamental developments and applications in reacting flows, Prog. Energy Combust. Sci. 36 (2010) 280–306.
[49] A.F. Kapustinskii, Lattice energy of ionic crystals, Q. Rev. Chem. Soc. 10 (1956) 283–294.
[50] W.M. Haynes (Ed.), CRC Handbook of Chemistry and Physics, CRC Press/Taylor & Francis, 2017 97th Edition (Internet Version).
[51] J.R. McCreary, R.J. Thorn, Enthalpy of sublimation of zinc and cadmium; correlation of $\Delta H°0$ vs $\Delta S°$; comparison of torsional and knudsen vapor pressures, J. Chem. Phys. 50 (1969) 3725–3733.
[52] J.A. Dean (Ed.), Lange's Handbook of Chemistry, McGraw-Hill, Inc, 1998 15th Ed.